The crystallization of polypropylene in multiwall carbon nanotube-based composites

Carlos Marco, Mohammed Naffakh, Marián A. Gómez, Gonzalo Santoro and Gary Ellis*

Departamento de Física e Ingeniería de Polímeros, Instituto de Ciencia y Tecnología de Polímeros, CSIC, c/ Juan de la Cierva, 3, 28006, Madrid, Spain.

Correspondence to: Gary Ellis; e-mail: gary@ictp.csic.es

ABSTRACT

The crystallization process of isotactic polypropylene (iPP) was studied under both dynamic and isothermal conditions for a series of multi-wall carbon nanotube (MWCNT) composites with nanotube concentrations between 0.1 – 1.0% by weight. The nucleation activity of the nanofillers was confirmed for both dynamic and isothermal crystallization, and was shown to be composition dependent. The effect of the nanofiller on the crystallization of iPP was discussed using the temperature coefficients obtained to determine the interfacial free energy and free energy of nucleation. The basal interfacial free energy decreased with respect to that of neat iPP by up to 15% for as little as 0.1% MWCNT, subsequently decreasing linearly with increasing nanotube concentration. This behavior is in line with the crystallization behavior of iPP with conventional nucleating agents.

INTRODUCTION

Isotactic polypropylene is one of the most important contemporary semicrystalline polymers with a wide range of applications where the mechanical properties are frequently modified by the addition of fillers or nucleating agents [1-5]. The use of carbon nanotubes (CNTs) as fillers in polymeric nanocomposites has received much attention [6, 7] notably due to their unique structure, with a high aspect ratio and extraordinary mechanical properties, making them very attractive candidates for polymeric materials reinforcement [8-11]. A number of different studies have been undertaken in order to evaluate the influence of CNT fillers on the rheological, mechanical and electrical properties of iPP [12-23]. In iPP composites, factors such as the microstructure and degree of crystallinity, the crystallization rate and the crystalline morphology are considerably influenced by the presence of nanofillers or reinforcements present in the polymeric matrix. The understanding and control of these parameters related to the crystalline solid state of iPP is fundamental for the design of its properties.

Recently there has been a growing interest in the influence of CNTs on the crystallization behavior of iPP, both with regard to their nucleating activity and the generation of polymorphic crystalline forms [24-30]. However, whilst the nucleation activity of multi-wall carbon nanotubes (MWCNTs) on the crystallization of iPP is known there is relatively little information in the literature on the influence of MWCNTs on the crystallization behavior of iPP [17, 23, 26, 31-38], and to date no contrasted information relating to the energetic parameters associated with nucleation in iPP under isothermal conditions is available. In order to analyze the properties of polypropylene blends and composites, a thorough understanding of the characteristics of the crystallization process, under both dynamic and isothermal conditions, is

fundamental, including the nucleation mechanisms and crystallization kinetics. For this reason the aims of the present work are, firstly to compare the crystallization behavior of iPP under the influence of a MWCNT nanofiller in both dynamic and isothermal conditions, and secondly, to analyze the temperature coefficients under isothermal crystallization and determine the interfacial free energy and free energy of nucleation involved in the nucleation process.

EXPERIMENTAL

Materials and processing

A commercial iPP was employed, ISPLEN® PP 070 G2M (Repsol-YPF, Móstoles, Spain) with a melt flow index of 10.0 g / 10 min (230ºC/2.16 kg) and a density of 0.902 g.cm^{-3}. The MWCNTs were grown by the arc discharge method [39] by Dr. W. Maser and Dr. A. Benito (Instituto de Carboquímica, CSIC, Zaragoza, Spain). The quality of the nanotubes was evaluated using Raman spectroscopy [40] based on the I_G/I_D ratio [41] where I_G is the integrated intensity of the G-mode (sp^2 carbon, ordered structure) centered at around 1575 cm^{-1} and I_D is that corresponding to the D-mode (sp^3 carbon, disorder or defect mode) centered at around 1280 cm^{-1}. From averaged Raman spectra an I_G/I_D ratio of 4.42 ± 0.01 was observed.

PP/MWCNT composites were prepared by melt blending using a Haake MiniLab Rheomex CTW5 co-rotating twin-screw extruder (Thermo Scientific, Madison, USA) with a volume of 7cm^3. With the aim of improving the dispersion of the nanotubes in the matrix, 25% by weight of iPP in powdered form, produced by cryogenic impact milling of granules using a SPEX Model 6770 Freezer Mill (SPEX CertiPrep Ltd, Stanmore, UK) was mixed with the corresponding concentration of MWCNTs to produce a powdered masterbatch for each composition. Each masterbatch

was then mixed with the iPP granules and introduced into the extruder. Recent improvements in this premixing methodology have been demonstrated to significantly enhance the thermal and mechanical properties of polymer-MWCNT composites [42] through improved dispersion. The following blending conditions were employed: screw speed = 100 rpm, temperature = 200 ºC, and processing time = 5 min. Four different compositions were prepared with 0.1%, 0.25%, 0.5% and 1% by weight of nanotubes. A sample of neat iPP was also prepared under the same conditions.

Characterization techniques

Dynamic crystallization experiments were undertaken in a Mettler TA-4000/DSC30 differential scanning calorimeter (Mettler-Toledo Intl Inc.), and the data obtained was evaluated using STAR^e 9.10 software. Aluminum capsules were used with sample weights of approximately 12 mg studied under an inert nitrogen atmosphere flow at a rate of 25 ml.min^{-1}. Several cooling cycles from the melt were undertaken at cooling rates, R, of 20, 10, 5 and 2 ºC.min^{-1}, followed by heating cycles at 5ºC.min^{-1} over the interval of temperatures between 30 and 210ºC. The melting temperature, T_m, and the crystallization temperature, T_p, were determined at the maximum of the melting endotherm observed during the heating scan and the minimum of the crystallization exotherm observed during the cooling scan, respectively. The elimination of the thermal history prior to the crystallization of polypropylene was achieved by maintaining the samples for five minutes at a residence temperature of 210ºC in the melt [43], in order to eliminate memory effects and to assure the maximum thermal stability of the components.

Isothermal crystallization was studied using a Perkin-Elmer DSC7/7700/UNIX differential scanning calorimeter (Perkin-Elmer España SL, Madrid, Spain), calibrated

with indium (T_m = 156.6 °C, ΔH_m = 28.45 kJ kg[1]) and zinc (T_m = 419.47 °C, ΔH_m = 108.37 kJ kg[1]). Once again, approximately 12 mg samples were weighed in aluminum capsules, and studied under a nitrogen gas flow of 25 ml min^{-1}. After the thermal history was erased prior to crystallization, as commented previously, the samples were cooled from the melt to each crystallization temperature, T_c , at a rate of 64 °C min^{-1}. The exotherm was subsequently registered as a function of time until crystallization was considered to be complete. The isothermal step was followed by a heating cycle up to 210 °C at a rate of 5 °C min^{-1}. The time associated with each degree of conversion, τ_i was obtained by integration of the corresponding crystallization exotherms. The crystallization rate, G, was analyzed using values of $\tau_{0.1}$, which correspond with the time required to reach a degree of crystalline conversion of 10%. If we consider that $G \sim (\tau_{0.1})^{-1}$, this parameter is representative of the overall crystallization rate for each crystallization temperature.

The apparent transition enthalpy, ΔH_{app} was determined from the area under the crystallization curve, taking the upper and lower limits in the corresponding deviations from the baseline. The conversion from apparent enthalpy to degree of crystallinity, *(1-λ)*, was calculated using the following equation:

$$(1-\lambda) = 100\left(\frac{\Delta H_{app}}{w\Delta H_m}\right) \tag{1}$$

where ΔH_m = 207.1 kJ kg^{-1}, corresponding to the melting enthalpy of 100% crystalline iPP [44], and w is the weight fraction of MWCNT.

X-ray diffraction experiments employing synchrotron radiation were undertaken at HASYLAB, in the DESY Synchrotron in Hamburg. Simultaneous measurements at wide angles, WAXS, and small angles, SAXS, were obtained in real time using the angular distribution of dispersed energy method employing a double focus camera

comprised of a Germanium Ge^{111} monochromator and a series of quartz focusing mirrors. The wavelength corresponding to the (111) plane of Ge^{111} is 0.15 nm. Linear Gabriel WAXS and SAXS detectors were used. The sample-to-detector distance for SAXS was 2.36 m and that for WAXS was 0.135 m, with the entire system maintained under vacuum conditions. The detectors were calibrated with standards; poly(ethylene terephthalate) in the case of WAXS, and RTT (rat tail tendon) in the case of SAXS. Film samples were prepared by compression and crystallization in a Mettler FP90/FP82 HT temperature cell (Mettler-Toledo Intl Inc.).

RESULTS AND DISCUSSION

Dynamic Crystallization

The crystallization exotherms of neat iPP and iPP in its respective binary composites, obtained in dynamic conditions by cooling from the melt, were observed to shift to lower temperatures and broaden as the cooling rate was increased. This is directly related to the formation of smaller crystals with a wider distribution of crystallite sizes. Figure 1 shows crystallization exotherms of neat iPP and the iPP/MWCNT composites at a cooling rate of 10 $°C.min^{-1}$ where a marked shift to higher T_p values can be observed. In Figure 2 the variation of T_p with concentration of MWCNT for neat iPP and all the materials analyzed is given. T_p is affected by the presence of the nanotubes at all cooling rates, for example, a significant increase of around 6°C in this parameter with 0.1% MWCNT can be observed at a cooling rate of 10$°C.min^{-1}$. At higher MWCNT concentrations the value of T_p for iPP continues to rise and tends to stabilize for the highest concentrations of 0.5 y 1%, where increments of around 8°C in the value of T_p were registered, Table 1. This effect on the crystallization of iPP in the composites must be attributed to a crystalline induction effect by the

MWCNTs that favors the nucleation stage of iPP, and consequently increases the crystallization rate, and is manifested by a higher crystallization temperature than neat iPP for the same cooling rate. These results are in agreement with those described recently for iPP/MWCNT nanocomposites prepared from the melt with concentrations between 0.5 - 5% by weight of MWCNT [17, 23, 26, 35, 38-45]. The levels of crystallinity developed during the cooling cycles, and the values obtained for T_m in the heating cycle subsequent to crystallization, were practically identical for both neat iPP and the nanocomposites. This observation is consistent with some of the results observed in the literature [16, 25, 33].

Under the previously described dynamic crystallization conditions, iPP crystallized in the α, or monoclinic form. The WAXS diffractograms of the binary iPP/MWCNT composites, Figure 3a, only present reflections associated to the crystalline planes characteristic of the monoclinic polymorph of iPP [46].

With a view to analyzing the possible variations in the lamellar structure of polypropylene room temperature SAXS diffractograms were measured for all samples after the dynamic crystallization from the melt at 10ºC.min^{-1}, Figure 3b. The long spacing, L, calculated from the reciprocal of the maximum scattering value, s_{max}, obtained from the Lorenz corrected intensity profile, increased from a value of 10 nm for neat iPP to 13 nm for the 1% MWCNT nanocomposite, Table 1. If one takes into account the reproducibility of the melting temperature of iPP in the nanocomposites with respect to that of neat iPP commented previously, it seems more reasonable to associate the variations observed in the long spacing to the possible location of the nanotubes in the interlamellar spacings rather than to an increase in the size of the iPP crystallites. It seems evident that during the crystallization process a migration of the MWCNTs from the lamellar growth front must take place as they are progressively

excluded from the crystals, generating aggregates that are located either in the interspherulitic spaces, in the interphase regions of the crystalline lamellae, or in the amorphous regions of the lamellar stacks. These previously commented results agree with recent work on iPP/MWCNT nanocomposites with 1 y 2% of nanotubes prepared from xylene solutions [34].

The evolution of the crystallization process from the melt state to the organized state was studied by following the variation in conversion, or the percentage of crystalline transformation, as a function of temperature for the various cooling rates analyzed. The tendency shown by the conversion curves, with a much accelerated primary crystallization even at the lowest cooling rates, did not allow the application of the Ozawa treatment for the analysis of non-isothermal crystallization kinetics [47].

On the other hand, when we take into account the variation in the crystallization temperature, considered as the minimum in the T_p with R, it is possible to estimate the nucleating activity of the MWCNTs, Φ, using the method developed by Dobreva y Gutzow [48], where the relationship between the undercooling of the system on crystallization, ΔT_p and the crystallization rate is given by:

$$log\ R = A - (B/2.303\Delta T_p^{\ 2}) \tag{2}$$

for the case of homogeneous nucleation, and by:

$$log\ R = A - (B^*/2.303\Delta T_p^{\ 2}) \tag{3}$$

for heterogeneous nucleation, where $\Delta T_p = T_m - T_p$.

If we consider that when crystallization takes place in a temperature range relatively close to the melting temperature, the potential barrier for crystalline growth is much smaller than that corresponding to the crystalline nucleation process. Thus, crystallization will be governed by the crystalline nucleation stage, and the nucleation activity is given by:

$$\Phi = B^*/B \qquad (4)$$

which can be obtained from the gradients of eq. 2 and 3. This nucleation efficiency is directly related with the energy of adhesion between the nucleating substrate and the nucleated crystalline phase, β, by the expression:

$$\Phi = 1 - (\beta/2\sigma) \qquad (5)$$

where σ is the specific surface energy at the crystalline interface. When $\beta \to 2\sigma$, $\Phi \to 0$, and the nucleating activity tends to its optimum, whilst on the contrary, when $\beta \to 0$, $\Phi \to 1$, and the nucleation activity tends to zero, as occurs in the case of homogeneous nucleation. In Figure 4, eq. 2 and 3 are represented for neat iPP and the compounds analyzed, considering a value of 210ºC for the thermodynamic equilibrium melting temperature of iPP [49]. The values of Φ obtained oscillate between 0.88 for a MWCNT concentration of 0.1% to 0.77 for a concentration of 1.0%.

The nucleation efficiency can also be determined from the variation observed in the crystallization temperature of the iPP matrix in the MWNT nanocomposites with respect to that found in the same matrix by an auto nucleation process at the same cooling rate. In this situation, the concentration and distribution of crystalline nuclei and the nucleus-matrix interaction can be considered ideal, and the nucleation efficiency should be at its maximum [50, 51]. Given that the two extremes in the efficiency scale are the non-nucleated matrix and the auto nucleated matrix, the nucleation efficiency, NE, can be expressed as:

$$NE = 100(T_{p\_}T_{pl})/(T_{al} - T_{pl}) \qquad (6)$$

where T_{al} y T_{pl} are the temperatures of crystallization associated with the non-nucleated and auto nucleated matrix, respectively. Considering a value of $T_{pl} = 140$ ºC [52], values for NE from 27% to 36% were obtained for MWCNT concentrations between 0.1% and 1.0%, for a cooling rate of 10ºC/min. In Figure 5, the evolution of both the

nucleating activity and the nucleating efficiency are compared as a function of the concentration for the PP/MWCNT composites analyzed in this work.

Isothermal crystallization

The isothermal crystallization behavior of neat iPP has been analyzed over a crystallization temperature range between 126 and 133°C. Figure 6a shows the evolution of the crystallization exotherms of neat iPP. As the crystallization temperature increased, the exotherms shifted along the time axis. Both the induction time and the width of the exotherms increased, which reflects a reduction in the crystallization rate with decreasing undercooling of the system, ΔT. The isothermal crystallization behavior of iPP in the nanocomposites was analyzed over the crystallization temperature range between 132 and 144 ºC. In this case, the crystallization exotherms of iPP presented shorter induction times and a narrower integral area than those corresponding to neat iPP, and showed an apparent increase in the isothermal crystallization rate, Figure 6b for the case of iPP/MWCNT 0.25%. This behavior was generalized and occurred over the whole composition range analyzed.

The rate of crystallization, G, was analyzed using the values of $\tau_{0.1}$ which corresponds to the time necessary to reach a degree of crystalline transformation of 10%. This parameter represents the global crystallization rate for each crystallization temperature considering that $G \sim (\tau_{0.1})^{-1}$. A pronounced change in the crystallization rate was be observed as the temperature increased, in other words, as the undercooling decreased, Figure 7. Also the apparent increase in the isothermal crystallization rate of iPP on the addition of MWCNT in the binary nanocomposites, shown previously by comparison of the crystallization exotherms, was now exhibited over the full

11

temperature range analyzed. Thus, it can be deduced that the nanofiller produced a nucleating effect on the crystallization of iPP.

A saturation effect of the nucleating activity of the MWCNTs on iPP has been described recently in the literature for MWCNT concentrations between 0.2 - 1.0% by weight [53]. Also, confinement effects on the polymer chains in the crystallization of nylon-6,6 in the presence of MWCNTs have been reported by Li *et al* [54]. Neither of these effects have been observed in the present work.

The crystallization kinetics was analyzed using the Avrami and Göler-Sachs models [55]. The Avrami model takes into account the perturbation of adjacent crystalline nuclei in the crystallization process, and the Göler-Sachs model assumes free crystalline growth. The Avrami model can be represented in the following manner:

$$\ln(1 - \theta) = kt^n \qquad (7)$$

where θ is the degree of crystalline conversion, k is the rate constant and n is the Avrami exponent that reflects the mode of crystalline nucleation and growth. In Figure 8 the variation in the crystalline conversion as a function of time is given for neat iPP and the iPP/MWCNT 0.25% composite. From these data, by the application of the Avrami model for each crystallization temperature over the temperature range analyzed, considering a crystalline transformation under 25%, values of the Avrami exponent, $n \approx$ 3 were determined in all cases. This value implies a three-dimensional heterogeneous crystal growth that is practically unchanged with the addition of MWCNT. Values of n $\approx$ 3 have also been found for some iPP/SWCNT composites [25], and values between 2 and 3 for both iPP/SWCNT [24, 30], and iPP/MWCNT composites [34, 35].

The determination of this parameter allowed the analysis of the overall crystallization rate of the crystallization process from the rate constant, k, at each crystallization temperature by the following expression [56]:

$$k = \frac{\ln 2}{\tau_{0.5}^n} \qquad (8)$$

where $\tau_{0,5}$ is the time needed to reach 50% crystalline transformation. Values of k obtained for each composite and crystallization temperature are given in Table 2. For example, at a T_c of 133ºC, the values of k can be observed to vary from 1.5×10^{-4} min^{-1} for neat iPP, to 6.5×10^{-2} min^{-1} for the composition with 0.5% by weight MWCNT. These results confirm the nucleating activity of the MWCNT on the crystallization of iPP in isothermal conditions. There is only one antecedent in the literature that presents values for the rate constant in iPP/MWCNT compounds [35]. These were determined by extrapolation from the Avrami expression under isothermal crystallization conditions at much higher undercoolings than those employed in the present work, and variations in the values of k were reported between $1.5.10^{-7}$ s^{-1} and $1.8.10^{-4}$ s^{-1} for neat iPP and the composite with 1% MWCNT, respectively [35]. Hardly any k-value data have been published for nanocomposites of iPP with SWCNT [25, 30].

Melting behavior after isothermal crystallization

After isothermal crystallization at different crystallization temperatures, the nanocomposites were heated at 5 ºC min^{-1} to the molten state. The melting behavior of neat iPP showed a single endotherm with a well defined maximum, T_mI, and some asymmetry in the lower temperature region, where shoulders, T_mII, appeared for the higher crystallization temperatures, Figure 9a. Both the main endothermic maximum and the associated lower temperature shoulder shifted to higher temperatures with increasing crystallization temperature, T_c. This is related to the formation of crystals whose sizes increase with the reduction in the degree of undercooling. The shift of both endotherms with increasing T_c suggests the existence of partial crystal size segregation in the isothermally formed crystallites. The smaller crystals generated the lower

temperature shoulders, and the enthalpy contribution of the melting of the larger more perfect crystals was included in the higher temperature endotherm. However, a contribution from the melting-recrystallization-melting of more imperfect crystals cannot be ruled out [45, 57].

From the analysis of the wide angle X-ray diffractograms recorded under isothermal crystallization conditions, only reflections associated with the monoclinic structure of iPP were detected. No evidence of the fundamental crystalline reflection at $2\theta = 16.2°$ corresponding to the (3,0,0)-plane of the trigonal structure [45] was observed.

The presence of the MWCNT does not substantially modify the melting behavior of iPP. In Figure 9b-c the double endotherm phenomenon was still observed for compositions of 0.1 and 0.25% MWCNT, but in these cases there was a clear increase in the values of T_mII and T_mI with respect to the melting of neat iPP as a consequence of the formation of the crystallites at higher crystallization temperatures, i.e. at smaller undercooling.

Temperature coefficient

When polymeric materials are crystallized with low undercooling, i.e. high crystallization temperatures, the crystallization rate is higher the greater the undercooling. This implies that the crystallization process is controlled by the nucleation stage, i.e. by the free energy needed for the formation of a stable crystallite or the free energy of nucleation, ΔG^*.

In agreement with the kinetic theory of crystallization [58-60], independent of the type of regime, the crystallization rate G can be given by:

$$\log G + \left[\frac{U}{2.3R(T_c - T_\infty)} \right] = \log G_0 - \left(\frac{K_{g(III)}}{2.3T_c \Delta T} \right) \qquad (9)$$

where $K_{g(III)} = 4\ \sigma_u \sigma_e b_0 T_m^0\ /\ k\ \Delta H_m$ for Regime III [61-64], k being the Boltzmann constant, 1.38×10^{-26} kJ K^{-1}, $b_0 = 6.26$ Å, represents the thickness of a crystalline monolayer added during growth, σ_e and σ_u are the basal and lateral interfacial free energies of the crystallite, respectively, and $U/2.3R(T_c-T_\infty)$ represents the transport term through the liquid – crystal interface at the crystallization temperature T_c [65]. The temperature T_∞ is that at which the viscosity of the system is infinite, and is equivalent to the value $T_g - 30$ which is 231.1 K for polypropylene. The parameter U is variable, and a value of 6.270 kJ kmol^{-1} is generally adopted. The representation of the first term of equation 8 versus $1\ /\ 2.3\ R\ T_c\ \Delta T$ is presented in Figure 10 for all of the samples analyzed.

The literature values for ΔH_m are both variable and dispersed and are fundamentally conditioned by the method of determination [46]. However, it is possible to eliminate the influence of this parameter in the comparative analysis of the values of the interfacial free energies by applying the approximation of Hoffman, Davis and Lauritzen [58], which establishes that the interfacial free energy can be given by the following expression,

$$\sigma_u = \alpha \Delta H_m \left(a_0 b_0 \right)^{1/2} \qquad (10)$$

where $\alpha \approx 0.1$ and $a_0 b_0 = 34.37$ Å^2 which represents the chain cross section in the iPP crystal, and the values of the basal interfacial free energy can be obtained from the following expression:

$$\sigma_e = \frac{k K_{g(III)}}{4 b_0 T_m^0 \alpha \left(a_0 b_0 \right)^{1/2}} \qquad (11)$$

Under these considerations, the values obtained for the basal interfacial free energy were 1.38, 1.32, 1.28 and 1.15x10^{-8} kJ cm^{-2} for 0.1, 0.25, 0.5 and 1% MWCNT, respectively. From the data obtained in this work, it seems evident that the reduction in the values of σ_e in the binary iPP/MWCNT composites, compared to the value of 1.61x10^{-8} kJ cm^{-2} in the case of neat iPP, was associated with the nucleating effect of the MWCNT, in agreement with Beck [66], and are similar to those which occur in the presence of nucleating agents [67-70] , nanofillers [71], or different types of fibers where transcrystallization is observed [49,72]. Recently Razavi-Nouri *et al.* [73] observed a progressive decrease in the basal interfacial free energy associated with the isothermal crystallization of iPP in PP-SWCNT composites up to a nanotube concentration of 0.5%. However, to our knowledge, the values in the literature for σ_e in the isothermal crystallization of iPP in composites with MWCNTs is very scarce. Only Zhou *et al*. [36] have reported a value of 1.1x10^{-8} kJ.cm^{-2} for neat iPP, increasing to 1.4x10^{-8} kJ.cm^{-2} in the presence of 0.5% MWCNT with a subsequent reduction to 0.75x10^{-8} kJ.cm^{-2} for 1% MWCNT. However, no justification for this variation with respect to the nucleation activity of the nanotubes is given.

It is accepted that the presence of a foreign substrate in the iPP melt frequently reduces the critical size of the crystalline nucleus necessary for subsequent growth, since the generation of an interphase between the polymeric crystal and the substrate may be less restricted than the creation of a crystalline nucleus from the melt [74]. As a matter of fact, heterogeneous nucleation occurs through the reduction of the free energy of nucleation, which gives rise to a higher nucleation rate and, as such, a higher crystallization rate.

The free energy of nucleation, i.e. the free energy necessary for the formation of a nucleus of a critical size, is given by the expression,

$$\Delta G* = \frac{4b_0\sigma_u\sigma_e T_m^0}{\Delta H_m \Delta T} \qquad (12)$$

$\Delta G*$, which increases with smaller undercooling, was lower for the iPP/MWCNT composites than for neat iPP at the same crystallization temperature, Figure 11, which confirms that the energy barrier for nucleation is lowered in the presence of the MWCNT component, leading to an increase in the overall crystallization rate.

It is clear that the viscosity of the iPP melt increases with the concentration of MWCNT, and consequently the energy required to transport the polymeric chains to the growing crystalline lamellae also increases. This increase in the transport energy, which is opposed to the increase in the overall crystallization rate, is mitigated by the reduction in the free energy of nucleation which favors the crystallization process, such that the resulting balance in the process is an increase in the rate of crystallization with increasing MWCNT content over the concentration range studied.

CONCLUSIONS

The analysis of the crystallization of iPP in its composites with MWCNTs by differential scanning calorimetry, under both isothermal and dynamic conditions, has demonstrated that both the crystallization temperature of iPP obtained under dynamic conditions and the isothermal crystallization rate are affected by the presence of MWCNT, showing a significant increase in both parameters. This is composition dependent and confirms the existence of a nucleation effect on the crystallization of iPP due to the presence of MWCNT dispersed in the iPP melt. This nucleation phenomenon is manifested by a reduction in the values of basal interfacial free energies for iPP, and a subsequent reduction in the free energy of nucleation and an increase in the global crystallization rate, whilst maintaining the monoclinic crystalline structure of iPP. The

17

presence of MWCNTs only has a slight influence on the double-endothermic melting behavior of iPP, manifesting small but clear increments in the melting temperatures.

REFERENCES

1. X. Liu and Q. Wu, *Polymer* **42**, 10013 (2001)

2. W. Qiu, K. Mai and H. Zeng, *J. Appl. Polym. Sci.*, **77**, 2974 (2000)

3. E. Assouline, S. Pohl, R. Fulchiron, J.F. Gerard, A. Lustiger, H.D. Wagner and G. Marom, *Polymer* **41**, 7843 (2000)

4. C. Marco, G. Ellis, M.A. Gómez and J.M. Arribas, *Recent Res. Devel. Appl. Pol. Sci.*, **1**, 587 (2002)

5. W. Su, M. Ge and P. He, *J. Polym. Sci. Polym. Phys.*, **40**, 408 (2002)

6. H.D. Wagner, O. Lourie, Y. Feldman and R. Tenne, *Appl. Phys. Lett.*, **72**, 188 (1998)

7. R. Dagani, *Chem. Eng. News* **77**, 25 (1999)

8. L.S. Schadler, S.C. Giannaris and P.M. Ajayan, *Appl. Phys. Lett.*, **73**, 3842 (1998)

9. F.T. Fischer, R.D. Bradshaw and L.C. Brinson, *Appl. Phys. Lett.*, **80**, 4647 (2002)

10. S. Curran, P. Ajayan, W. Blau, D. Carrol, J. Coleman, A. Dalton, A.P. Davey, B. McCarthy and A. Stevens, *Adv. Mat.*, **10**, 1091 (1998)

11. M. Alexandre and P. Dubois, *Mat. Sci. Eng.*, **28**, 1 (2000)

12. T. Kashiwagi, E. Grulke, J. Hilding, K. Groth, R. Harris, K. Butler, J. Shields, S. Kharchenko and J. Douglas, *Polymer* **45**, 4227 (2004)

13. T.E. Chang, L.R. Jensen, A. Kisliuk, R.B. Piper, R. Pyrz and A.P. Sokolov, *Polymer* **46**, 439 (2005)

14. K. Lozano and E.V. Barrera, *J. Appl. Polym. Sci.*, **79**, 125 (2001)

15. S. Kumar, H. Doshi, M. Srinivasarao, J.O. Park and D.A. Schiraldi *Polymer* **43**, 1701 (2002)

16. W.E. Dondero and R.E. Gorga, *J. Polym. Sci. Polym. Phys.*, **44**, 864 (2006)

17. Z. Zhou, S. Wang, Y. Zhang and Y. Zhang, *J. Appl. Polym. Sci.*, **102**, 4823 (2006)

18. J.C. Kearns and R.L. Shambaugh, *J. Appl. Polym. Sci.*, **86**, 2079 (2002)

19. S.H. Lee, H.W. Kim, S.H. Kim and J.R. Youn, *Eur. Polym. J.*, **44**, 1620 (2008)

20. P. Zhao, K. Wang, H. Yang, Q. Zhang, R. Du and Q. Fu, *Polymer* **48**, 5688 (2007)

21. Y. Xiao, X. Zhang, W. Cao, K. Wang, H. Tan, Q. Zhang, R. Du and Q. Fu, *J. Appl. Polym. Sci.*, **104**, 1880 (2007)

22. M. GamB, B.K. Satapathy, M. Thunga, R. Weidisch, P. Pötschke and A. Janke, *Makromol. Rapid Commun.*, **28**, 1624 (2007)

23. H. Zhang and Z. Zhang, *Eur. Polym. J.*, **43**, 3197 (2007)

24. B.P. Grady, F. Pompeo, R.L. Shambaugh and D.E. Resasco, *J. Phys. Chem. B*, **106**, 5852 (2002)

25. A.R. Bhattacharyya, T.V. Sreekumar, T. Liu, S. Kamar, L.M. Ericson, R.H. Hauge and R.E. Smalley, *Polymer* **44**, 2373 (2003)

26. E. Assouline, A. Lustiger, A.H. Barber, C.A. Cooper, E. Klein, E. Wachtel and H.D. Wagner, *J. Polym. Sci. Polym. Phys.*, **41**, 520 (2003)

27. L. Valentine, J. Biagiotti, J.M. Kenny and S. Santucci, *Compos. Sci. Tech.*, **63**, 1149 (2002)

28. E.M. Moore, D.L. Ortiz, V.T. Marla, R.L. Shambaugh and B.P. Grady, *J. Appl. Polym. Sci.*, **93**, 2926 (2004)

29. L. Valentine, J. Biagiotti, J.M. Kenny and S. Santucci, *J. Appl. Polym. Sci.*, **87**, 708 (2003)

30. L. Valentine, J. Biagiotti, M.A. López Manchado, S. Santucci and J.M. Kenny, *Polym. Eng. Sci.*, **44**, 303 (2004)

31. J. Sandler, G. Broza, M. Nolte, K. Schulte, Y.M. Lam and M.S.P. Shaffer, *J. Macromol. Sci. Phys*., **B42**, 479 (2003)

32. H.S. Xia, Q. Wang, K.S. Li and G.H. Hu, *J. Appl. Polym. Sci*., **93**, 378 (2004)

33. M.V. Jose, D. Dean, J. Tyner, G. Price and E. Nyairo, *J. Appl. Polym. Sci*., **103**, 3844 (2007)

34. C.A. Avila Orta, F.J. Medellín-Rodríguez, M.V. Dávila Rodríguez, Y.A. Aguirre Figueroa, K. Yoon and B.S. Hsiao, *J. Appl. Polym. Sci*., **106**, 2640 (2007)

35. M.K. Seo, J.R. Lee and S.J. Park, *Mat. Sci. Eng*., **A404**, 79 (2005)

36. Z. Zhou, S. Wang, L. Lu, Y. Zhang and Y. Zhang, *J. Polym. Sci. Polym. Phys*., **45**, 1616 (2007)

37. K. Wang, C. Tang, P. Zhao, H. Yang, Q. Zhang, R. Du and Q. Fu, *Macromol. Rapid Commun*., **28**, 1257 (2007)

38. D. Wu D, Y. Sun, L. Wu and M. Zhang, *J. Appl. Polym. Sci.*, **108**, 1506 (2008)

39. A.M. Benito, W.K. Maser, M.T. Martínez, *Int. J. Nanotech.*, **2**, 71 (2005)

40. Signal-averaged Raman spectra were recorded at a spectral resolution of 4 cm^{-1} on a Perkin Elmer System 2000-R Fourier transform Raman spectrometer, with a Nd^{3+}:YAG laser source (200 mW incident on the sample), and a room temperature InGaAs detector.

41. M. S. Dresselhaus, G. Dresselhaus, A. Jorio, *J. Phys. Chem. C*, **111**, 17887 (2007)

42. G. Santoro, M.A. Gómez, C. Marco, G. Ellis, *Macromol. Mater. Eng.,* **295**, 652 (2010)

43. C. Marco, G. Ellis, M.A. Gómez and J.M. Arribas, *J. Appl. Polym. Sci*., **84**, 2440 (2002)

44. H.S. Bu, S.Z.D. Chang and B. Wunderlich, *Makromol. Chem. Rapid. Commun*., **9**, 76 (1988)

45. M. GamB, B.K. Satapathy, M. Thunga, R. Weidisch, P. Pötschke and J. Jehnichen, *Acta Mater*., **56**, 2247 (2008)

46. J. Karger-Kocsis, J. *Polypropylene: Structure, Blends and Composites,* Chapman & Hall (1995) New York

47. T. Ozawa, *Polymer* **12**, 150 (1971)

48. A. Dobreva and I. Gutzow, *J. Non-Cryst. Solids* **162**, 13 (1993)

49. R. Bouza, C. Marco, G. Ellis, Z. Martín, M.A. Gómez and L. Barral, *J. Therm. Anal. Cal*., **94**, 119 (2008)

50. B. Fillon, B. Lotz, A. Thierry and J.C. Wittmann, *J. Polym. Sci. Polym. Phys*., 31, 1395 (1993)

51. B. Fillon, A. Thierry, B. Lotz and J.C. Wittmann, *J. Therm. Anal. Cal*., 42, 721 (1994)

52. C. Marco, M.A. Gómez, G. Ellis and J.M. Arribas, *J. Appl. Polym. Sci*., **84**, 1669 (2002)

53. D. Xu and Z. Wang, *Polymer* **49**, 330 (2008)

54. L.Y. Li, C.Y. Li, C.Y. Ni, L.X. Rong and B. Hsiao, *Polymer* **48**, 3452 (2007)

55. L. Mandelkern, *Crystallization of polymers*, 2ⁿᵈ Ed., Vol. I. *Equilibrium concepts*, Cambridge University Press, Mc Graw Hill (2002)

56. S.H. Kim, S.W. Park and W.S. Gil, *J. Appl. Polym. Sci*., **67**, 1383 (1998)

57. C. Marco, G. Ellis, M.A. Gómez, J.M. Arribas, *J. Appl. Polym. Sci*., **88**, 2261 (2003)

58. E.J. Clark and J.D. Hoffman, *Macromolecules* **17**, 878 (1984)

59. J.D. Hoffman, G.T. Davies and J.J. Lauritzen, *Treatise on Solid State Chemistry*, Vol.3, N.B. Hannay Ed., Plenum Press (1976), New York

60. J.D. Hoffman, *Polymer* **24**, 3 (1983)

61. A.O. Ibhadon, *J. Appl. Polym. Sci*., **71**, 579 (1999)

62. J.J. Janimak and S.Z.D. Cheng, *J. Polym. Eng.*, **10**, 21 (1991)

63. B. Monasse and J.M. Haudin, *Coll. Polym. Sci.*, **266**, 679 (1988)

64. E.B. Bond, J.E. Spruiell and J.S. Lin, *J. Polym. Sci. Polym. Phys.*, **37**, 3050 (1999)

65. J.D. Hoffman, L.J. Frolen, G.S. Ross G.S and J.J. Lauritzen, *J. Res. Natl. Bur. Stand.*, **79A**, 671 (1975)

66. H.N. Beck, *J. Appl. Polym. Sci.*, **19**, 371 (1975)

67. J. Menczel and J. Varga, *J. Therm. Anal. Cal.*, **28**, 11 (1983)

68. Y. Fena, X. Jin and J.N. Hay, *J. Appl. Polym. Sci.*, **69**, 2089 (1988)

69. J. Yin, S. Wang, Y. Zhang and Y. Zhang, *J. Polym. Sci. Polym. Phys.*, **43**, 1914 (2005)

70. C. Li, D. Zhang and Z. Li, *J. Appl. Polym. Sci.*, **85**, 2644 (2002)

71. J. Ma, S. Zhang, Z.Z. Qi, G. Li and H. Hu, *J. Appl. Polym. Sci.*, **83**, 1978 (2002)

72. C. Wang C and C.R. Liu, *Polymer* **40**, 289 (1999)

73. M. Razavi-Nouri, M. Ghorbanzadeh-Ahangari, A. Fereidoon, M. Jahanshahi, *Polym. Test.*, **28**, 46 (2009)

74. M. Mucha and Z.J. Krolikowski, *J. Therm. Anal. Cal.*, **74**, 549 (2003)

TABLES

Table 1. T_p and T_{10} values obtained for PP/MWCNT composites under dynamic crystallization cycles from the melt. Values of long spacing, L, calculated from SAXS measurements are included.

| % MWCNT | R (°C.min^{-1}) | | | | | | | | L (A) |
| | 20 | | 10 | | 5 | | 2 | | |
	T_{10} (°C)	Tp (°C)	T_{10} (°C)	Tp (°C)	T_{10} (°C)	Tp (°C)	T_{10} (°C)	Tp (°C)	
0	110.1	105.6	117.6	112.0	119.6	116.0	123.7	120.7	100
0.1	116.9	113.6	123.8	119.6	125.5	122.9	129.6	127.2	119
0.25	117.8	114.5	124.3	120.4	127.2	124.5	131.9	129.1	121
0.50	120.5	116.8	125.6	122.7	129.3	126.5	133.7	131.1	122
1	119.9	116.7	125.8	122.0	128.8	126.0	133.4	130.5	130

Table 2. Values of the isothermal rate constant k calculated from Equation 7.

| Tc (°C) | $k \cdot 10^5$ (min^{-n}) | | | | |
	$W_{MWCNT} = 0$	0.1	0.25	0.5	1
126	2020				
127	1052				
128	535				
129	258				
130	126				
131	78				
132	37	3370	5700	12295	
133	15	1645	2328	6512	
134		814	1169	2843	5699
135		374	555	1369	2843
136		186	265	667	1486
137		86	135	338	760
138		42	67	211	394
139		21	38	105	202
140		9	20	52	113
141		6	10		61
142					32
143					17
144					9

FIGURES
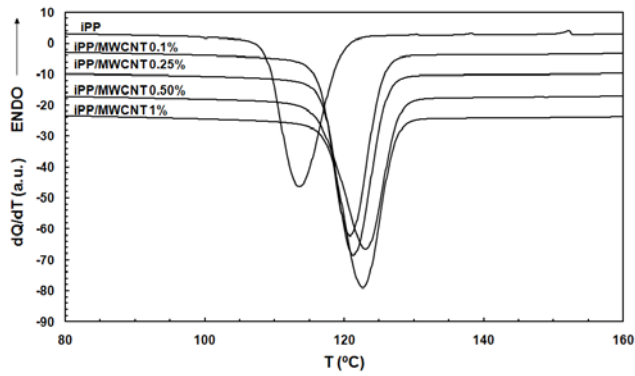
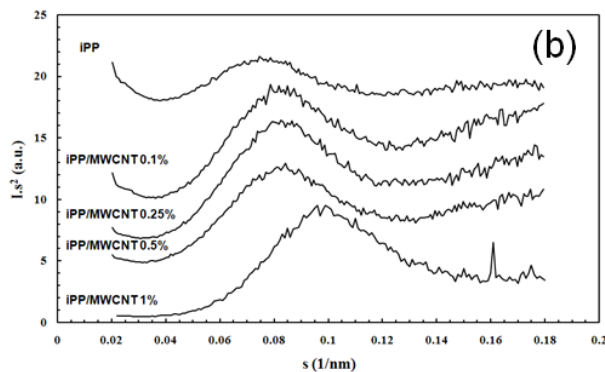
Figure 1. Crystallization exotherms recorded from the melt for iPP and its composite with MWCNT (concentrations shown) at a cooling rate of 10ºC.min^{-1}.
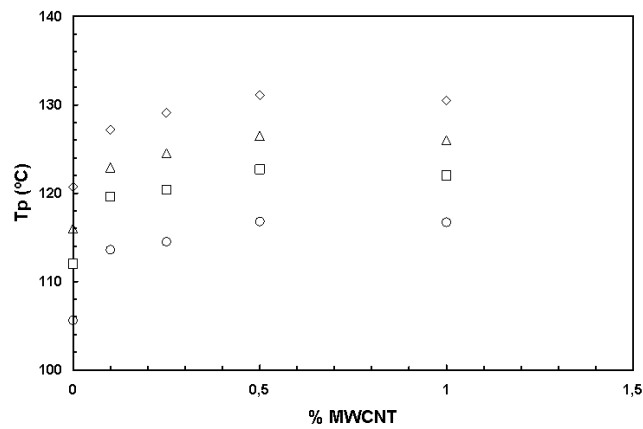
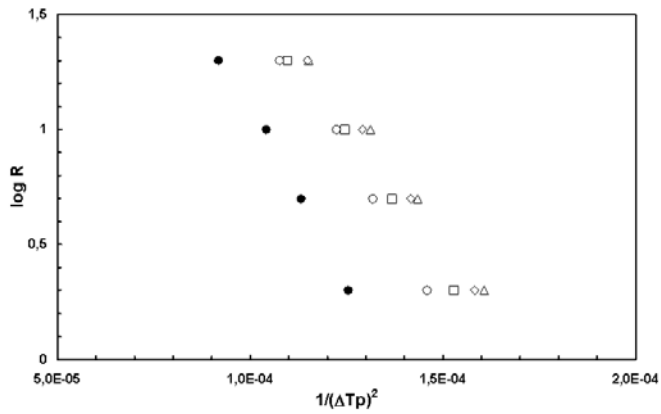**Figure 2.** Variation of the T_p values with MWCNT composition; ($\bigcirc$) 20ºC.min^{-1}, ($\square$) 10ºC.min^{-1}, ($\triangle$) 5ºC.min^{-1}, ($\diamondsuit$) 2ºC.min^{-1}.
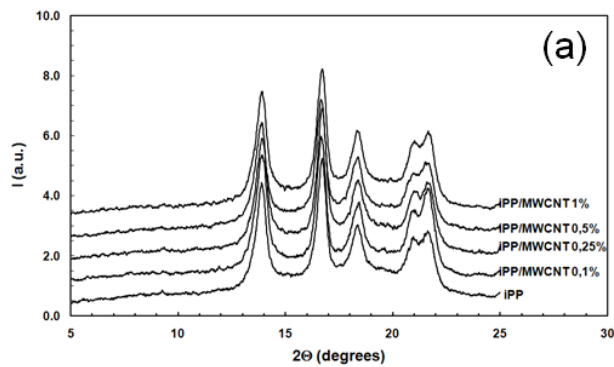
Figure 3. (a) WAXS and (b) SAXS diffractograms of iPP and iPP/MWCNT composites recorded at room temperature after crystallization from the melt at 10ºC.min^{-1}.

Figure 4. Plot of log R vs $1/\Delta T_p^2$, according the Dobreva´s approach. (●) iPP,(○) iPP/MWCNT 0.1%, (□) iPP/MWCNT 0.25%, (△) iPP/MWCNT 0.5%, (◇) iPP/MWCNT 1% .
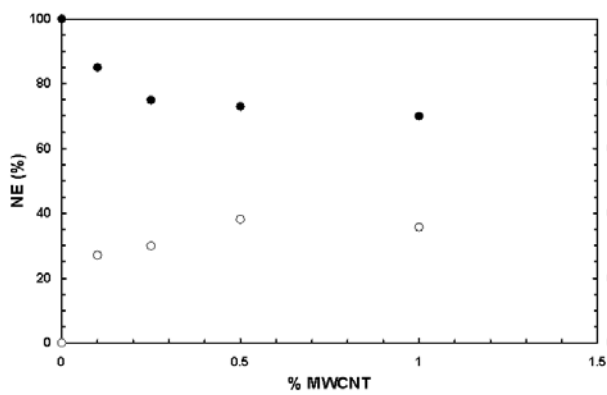

Figure 5. Variation of Φ (●) and NE (○), according the eq. 4 and 6, with MWCNT composition.
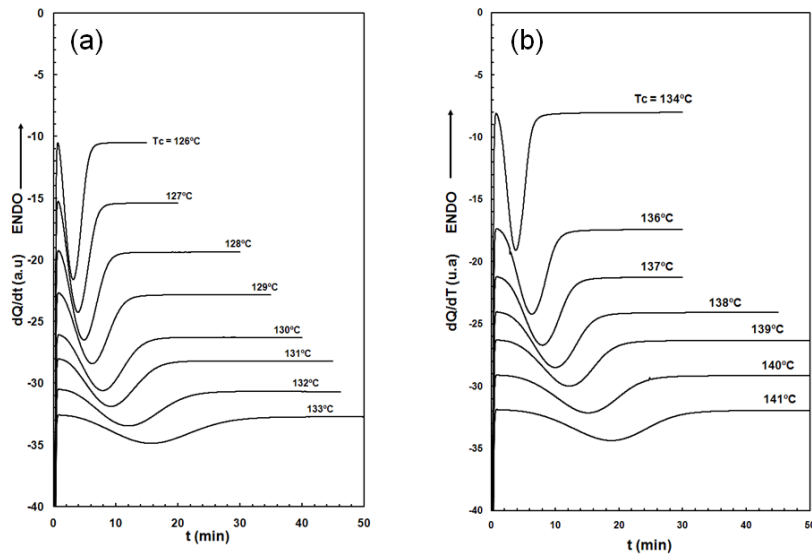
Figure 6. Crystallization exotherms for (a) raw iPP and (b) iPP/MWCNT 0.25%, under isothermal conditions at the indicated crystallization temperatures. The baselines are shifted along the ordinate axis (arbitrary units) for clarity.
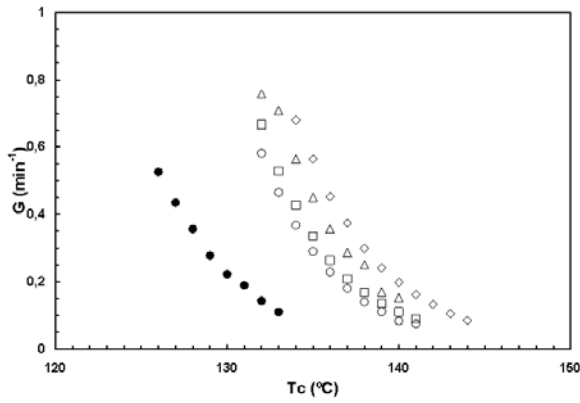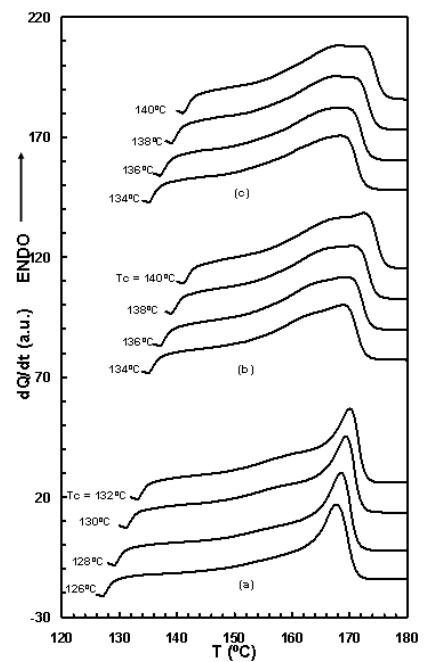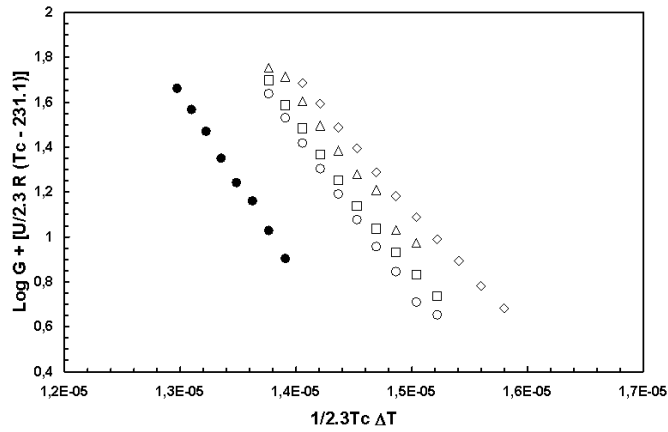
Figure 7. Variation in the isothermal crystallization rate, *G* with the crystallization temperature. (●) iPP,(○) iPP/MWCNT 0.1%, (□) iPP/MWCNT 0.25%, (△) iPP/MWCNT 0.5%, (◇) iPP/MWCNT 1% .
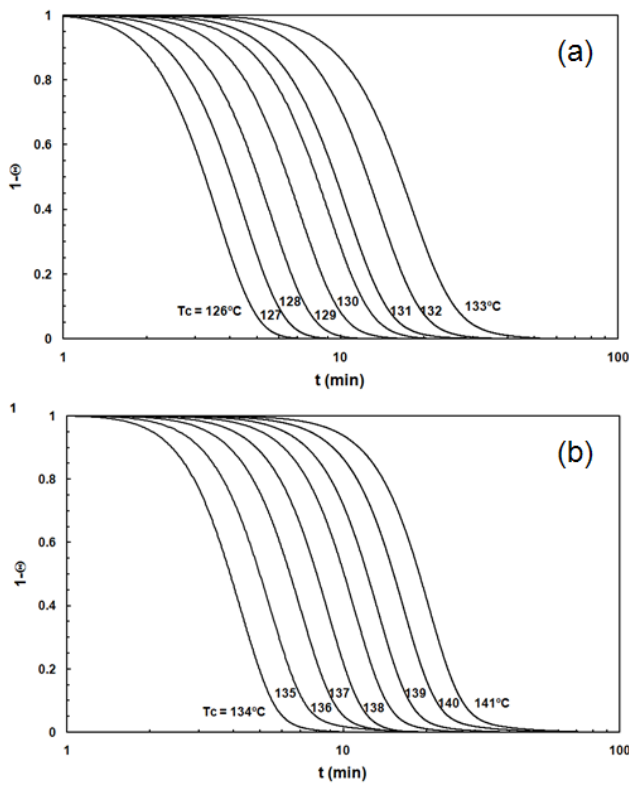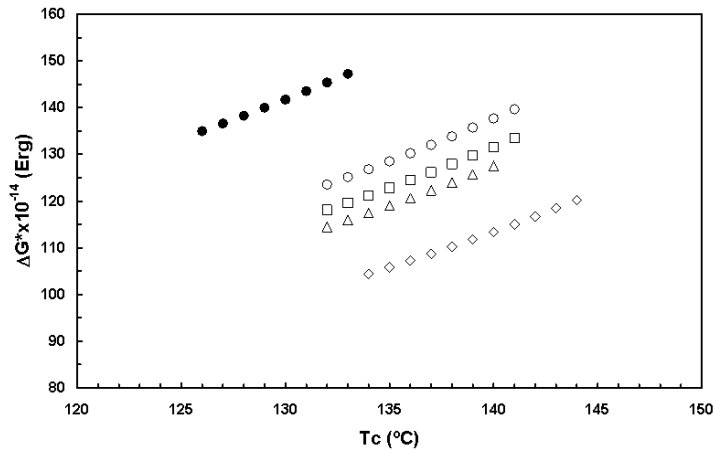

Figure 8. Variation in the crystalline conversion as a function of time is given for (a) neat iPP and (b) iPP/MWCNT 0.25% composite, at the indicated crystallization temperatures.

Figure 9. DSC thermograms for the heating cycle at 5 ºC.min⁻¹ of (a) iPP, (b) iPP/MWCNT 0.1% and (c) iPP/MWCNT 0.25% , after isothermal crystallization from the melt at the indicated crystallization temperatures. The baselines are shifted along the ordinate axis (arbitrary units) for clarity.

26

Figure 10. Temperature coefficient for all the materials studied, as determined by equation 8. (●) iPP,(○) iPP/MWCNT 0.1%, (□) iPP/MWCNT 0.25%, (△) iPP/MWCNT 0.5%, (◇) iPP/MWCNT 1%

Figure 11. Variation in the free energy of nucleation, ΔG^*, as a function of the crystallization temperature. (●) iPP,(○) iPP/MWCNT 0.1%, (□) iPP/MWCNT 0.25%, (△) iPP/MWCNT 0.5%, (◇) iPP/MWCNT 1%.